Catalysis Today 161 (2011) 181–188

Contents lists available at ScienceDirect

Catalysis Today

journal homepage: www.elsevier.com/locate/cattod

Photocatalytic oxidation of gaseous toluene on titania/mesoporous silica powders in a fluidized-bed reactor

Minoo Tasbihi[a], Urška Lavrenčič Štangar[a,*], Urh Černigoj[a,1], Jaromir Jirkovsky[b], Snejana Bakardjieva[c], Nataša Novak Tušar[d]

[a] Laboratory for Environmental Research, University of Nova Gorica, Vipavska 13, 5001 Nova Gorica, Slovenia
[b] J. Heyrovský Institute of Physical Chemistry, Academy of Sciences of the Czech Republic, Dolejškova 3, 128 23 Prague 8, Czech Republic
[c] Institute of Inorganic Chemistry ASCR v.v.i., 25069 Řež, Czech Republic
[d] Laboratory for Inorganic Chemistry and Technology, National Institute of Chemistry, Hajdrihova 19, 1000 Ljubljana, Slovenia

ARTICLE INFO

Article history:
Available online 19 September 2010

Keywords:
Titanium dioxide
Mesoporous silica
Photocatalysis
Toluene
Gas reactor

ABSTRACT

The photocatalytic degradation of toluene was carried out on titania/mesoporous silica photocatalysts in a self-constructed gaseous fluidized-bed photoreactor equipped with UVA light source. The powder photocatalysts were synthesized by incorporation of aqueous titania sol (as a photoactive component), into silica mesoporous materials (as a high-surface-area support), via the sol–gel impregnation method. SBA-15 was used as an ordered and KIL-2 as a disordered mesoporous silica support. The Ti/Si nominal molar ratio was adjusted to 1/2, 1/1 and 2/1. The photocatalysts were characterized by X-ray diffraction (XRD), nitrogen sorption (BET), UV–vis–NIR diffuse reflectance spectroscopy (DRS), Fourier transform infrared spectroscopy (FT-IR) and high-resolution transmission electron microscopy (HR-TEM). The effects of Ti/Si molar ratio and of the mesoporous silica structure were investigated measuring adsorption capacity and photocatalytic degradation of toluene. The rates of photocatalytic degradation reactions were found to be similar for photocatalysts with the same Ti/Si molar ratio independently of the mesoporous structure of silica. The adsorption capacity was decreasing as a function of the increasing Ti/Si molar ratio in the case of both types of mesoporous silica support. However, the photocatalytic degradation proceeded faster for the Ti/Si molar ratio 1/1 while, in the case of the other investigated Ti/Si molar ratios 1/2 and 2/1, the degradation rates were lower. In general, the photocatalytic activity was considerably improved by using supported titania–silica catalyst compared to an unsupported titania powder prepared from the same nanocrystalline titania sol.

1. Introduction

Emission of volatile organic compounds (VOCs) is one of the causes of indoor air pollution. The VOCs are common air pollutants and can be found in both outdoor and indoor environments [1,2]. Toluene was taken as a representative of VOCs for this study. Several strategies have been identified in order to reduce their presence in civil and industrial emissions. Among the methods for removing toluene from air, heterogeneous photocatalysis is one of the most attractive due to the mild experimental conditions [3–5].

Micro- and mesoporous molecular sieves are well established materials as catalysts and absorbents in many chemical and petrochemical processes [6]. These materials have large specific surface area, which causes a high adsorption capacity [7–9]. However, the treatment techniques based on adsorption only transfer the contaminant from air to another phase. Therefore, researchers have also investigated an activation of meso-ordered silica material with different metal or metal oxides such as titania (TiO_2) to destroy the VOCs pollutants chemically.

Titanium dioxide represents the most extensively used photocatalyst because of its high photocatalytic efficiency, stability towards photocorrosion and chemicals, no toxicity and low cost. The Ti-loaded mesoporous/nanoporous supports have some advantages in the photocatalysis such as: (1) formation of separated titania nanoparticles in the final composition, (2) increase of adsorption capacity especially for non-polar compounds, (3) lower scattering of UV irradiation [6].

Recently, various titania-containing mesoporous materials were synthesized for decomposition of toluene [6,10–13]. For example, Popova et al. [13] studied toluene oxidation on titanium species introduced into MCM-41 silica either by direct synthesis or by conventional impregnation procedure. They used propan-2-ol as

* Corresponding author. Tel.: +386 5 331 52 41; fax: +386 5 331 52 96.
E-mail addresses: minoo.tasbihi@ung.si (M. Tasbihi), urska.lavrencic@ung.si (U. Lavrenčič Štangar).
[1] Present address: BIA Separations d.o.o., Teslova 30, 1000 Ljubljana, Slovenia.

0920-5861/$ – see front matter © 2010 Elsevier B.V. All rights reserved.
doi:10.1016/j.cattod.2010.08.015

Table 1
Some physico-chemical characteristics, dark adsorption capacity and photocatalytic activity of the analyzed powders.

Sample	Ti/Si nominal molar ratio	Theoretical amount of TiO_2 in the powder (wt.%)	Crystallite size (nm)	S_{BET} ($m^2\ g^{-1}$)	Band gap (eV)	Dark adsorption capacity (% of adsorbed toluene)	Photocatalytic reaction rate constant k (min^{-1})
SBA-15	–	–	–	589	–	53	–
Ti/SBA-15(1/2)	1/2	40	–	560	3.39	20	0.0043
Ti/SBA-15(1/1)	1/1	58	–	498	3.20	16	0.0121
Ti/SBA-15(2/1)	2/1	74	12	336	3.14	8	0.0067
KIL-2	–	–	–	504	–	49	–
Ti/KIL-2(1/2)	1/2	40	–	345	3.26	17	0.0031
Ti/KIL-2(1/1)	1/1	58	5	309	3.17	14	0.0096
Ti/KIL-2(2/1)	2/1	74	7	296	3.15	9	0.0064
Ti1	–	73	8	80	3.11	9	0.0006
Millennium PC500	–	100	5–10	300	–	19	0.0114

a synthesis medium and titanium ions were incorporated as tetra-coordinated in the resulted structure.

In our recent work [14], ordered and disordered mesoporous silica supports were incorporated with different amounts of titania via the sol–gel impregnation method. Their adsorption capacity and photocatalytic activity were evaluated using iso-propanol as a model VOC. For this study, a gaseous photoreactor coupled on-line with an FT-IR spectrometer was employed. It was shown that the functional properties of the synthesized material depend on the titania source as well as on the type of silica support (either ordered mesoporous SBA-15 or disordered mesoporous KIL-2).

In this study, ordered mesoporous SBA-15 and disordered mesoporous KIL-2 silicate materials were functionalized by aqueous nanocrystalline titania sol via a sol–gel impregnation following our previous work [14]. We chose the aqueous nanocrystalline titania sol as the TiO_2 source for the following reasons: (1) nearly unchanged structure of the silica support after impregnation of titania sol (the structure was destroyed if using hydrolyzed titanium isopropoxide and heat treatment) and (2) a discovered enhancement of the photocatalytic performance of mesoporous silica functionalized by aqueous titania sol in a fixed-bed photoreactor [14]. For better understanding of the morphology and structural properties of the powders, the samples were characterized by Fourier transform infrared spectroscopy (FT-IR), UV–vis diffuse reflectance spectroscopy (DRS) and high-resolution transmission electron microscopy (HR-TEM) in addition to the techniques already employed in our previous work (XRD, N_2 sorption measurements, SEM, UV–vis–NIR) [14]. The adsorption capacity and photocatalytic activity of as-prepared powders were investigated by means of photocatalytic degradation of gaseous toluene in a fluidized-bed photoreactor, constructed for this purpose. The photocatalytic degradation of toluene was followed by on-line coupling of gas chromatography–mass spectrometry (GC–MS).

2. Experimental

2.1. Synthesis of titania/silica photocatalysts

Ordered mesoporous SBA-15 and disordered mesoporous KIL-2 silicate materials were used as high-surface-area supports. A detailed synthesis procedure for disordered mesoporous silica KIL-2 was reported in [15]. The ordered mesoporous silica SBA-15 powders were synthesized according to the procedure described in [14]. Also the procedure used for the incorporation of titania into the support was already described in detail in [14]. The aqueous crystalline anatase-TiO_2 sol was prepared from $TiCl_4$ as a titanium precursor and using $HClO_4$ as a peptizing agent with $[Ti]/[H^+]$ molar ratio equal to 2.5 [16]. This sol was deposited to the appropriate amount of SBA-15 or KIL-2 via the sol–gel impregnation method. Before impregnation, the pH of the sol was adjusted to 3 using 1 M NaOH solution resulting in a milky colloidal suspension. The pH adjustment was necessary to prevent destruction of the support in the case of reaction with a strong acid. Then a nominal amount of support was added to the colloidal dispersion. The mixture was stirred for 2 h at room temperature, followed by centrifugation and washing with deionized water until a pH of about 6 was reached. The resultant white precipitate was dried at 60 °C for 24 h. The samples prepared from KIL-2 and SBA-15 were designated as Ti/KIL-2(x) and Ti/SBA-15(x), respectively, where x means the Ti/Si nominal molar ratio that was adjusted to 1/2, 1/1 and 2/1.

For comparison, a TiO_2 powder was obtained from the same aqueous nanocrystalline TiO_2 sol by evaporation at 50 °C for 12 h followed by additional drying in air at 150 °C for 3 h [16]. This sample was denoted as Ti1. The commercial photocatalyst, a Millennium PC500 (100% anatase, BET surface area: 300 $m^2\ g^{-1}$, crystal size: 5–10 nm), was used as a reference photocatalyst. The theoretical amounts of titania (wt.%) in all samples are reported in Table 1.

2.2. Characterization

The X-ray powder diffraction (XRD) patterns were obtained on a PANalytical X'Pert PRO high-resolution diffractometer with an alpha 1 configuration using $CuK_{\alpha 1}$ radiation (1.5406 Å) with a step size of 0.033 using a fully opened X'Celerator detector. The average crystallite sizes were determined from the Scherrer's equation using the broadening of the (1 0 1) anatase peak reflection. The specific surface area was evaluated from nitrogen sorption isotherms obtained at 77 K by a Micromeritics Tristar 3000 instrument. The IR spectra of the samples dispersed in KBr pellets were recorded using a Perkin-Elmer FT-IR Spectrum 100 spectrometer with a 4 cm^{-1} resolution in the frequency range from 4000 cm^{-1} to 400 cm^{-1}. Diffuse reflectance spectra were measured on a Perkin-Elmer Lambda 19 UV–vis–NIR spectrophotometer equipped with an integrating sphere. The powders were placed in a 1 mm quartz cell. For the calculation of energy band gaps, the original coordinates of the spectra (reflectance vs. wavelength) were transformed to Kubelka–Munk function (K) vs. photon energy ($h\nu$) [17]. High-resolution transmission electron micrographs (HR-TEM) were obtained from a JEOL JEM 3010 microscope operated at 300 kV (LaB6 cathode, 1.7 Å point resolution) with an EDX (energy dispersive X-ray) detector attached. The powders were dispersed in water and a drop of diluted suspension was placed on a carbon-coated grid and evaporated at ambient temperature. Electron diffraction (ED) patterns were evaluated using the Process Diffraction software package.

2.3. Photoreactor set-up

The schematic diagram of the photoreactor system that was constructed for the photocatalytic experiments is shown in Fig. 1.

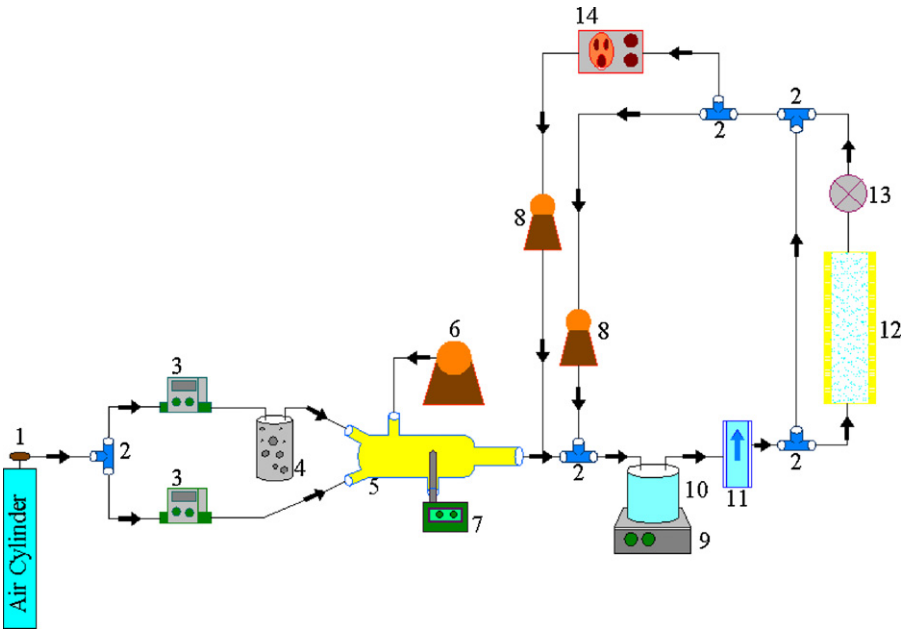

Fig. 1. Schematic diagram of the set-up for gaseous photocatalysis: (1) gas regulator, (2) 3-way valve, (3) mass flow meter/controller, (4) humidifier, (5) mixing chamber, (6) syringe pump, (7) thermometer and humidity meter, (8) diaphragm pump, (9) water bath, (10) reservoir vessel, (11) flow meter, (12) reactor cell with surrounding UVA lamps, (13) sampling port and (14) GC–MS.

The first part provides the feed for the reaction which consists of an air cylinder, mass flow meters/controllers (Aalborg AFC 26), a mixing chamber and a syringe pump (TSE System). The second part represents a reaction loop, which includes a flow meter (Aalborg), two compact diaphragm pumps (Sensortechnics GmbH), first for circulation of the mixed gas flow through the set-up and second for circulation of the mixed gas flow through the on-line GC–MS, a sampling port, a reactor cell, a 1 L reservoir vessel, a water bath (IKA, ET basic) and a chromatographic on-line GC–MS analyzer (Varian). Pure synthetic air (purity = 5.5) was used as a source of oxygen. The mixing chamber consists of a 30 cm long and of a 3 cm outer diameter Duran glass tube. The compact photoreactor (Rayonet reactor, model RPR-100) had dimensions of 35.5 cm × 35.5 cm × 20.5 cm. The reactor chamber consists of six low-pressure mercury fluorescent lamps which were used as a UVA radiation source (15 W, 265 mm × 16 mm, Philips CLEO; broad maximum at 355 nm) and the reflective surface of polished aluminum which is placed behind the lamps. An incident intensity of 36.5 W m^{-2} was determined at the photoreactor cell surface using photometry Xenocal UV-sensor. The reaction cell was made from a Duran glass tube (10 mm inner diameter, 27 cm height) and positioned vertically in the center of the photoreactor. A porous frit at the bottom of the reactor cell allowed distributing finely the inlet gaseous mixture through the catalyst powder. Another frit in the upper part of the reactor cell prevented the photocatalyst powders for escaping with the gas stream out of the photoreactor cell. All the connections, valves and tubes in this set-up were made of Teflon.

2.4. Photocatalytic experiments

In a typical test, the regulated air stream was divided into two paths. One served for the humidification of air and the other one transported dry air. The humidification was generated by bubbling air through a glass bottle containing deionized water. Both air flows were regulated by mass flow meters/controllers. The flow rates of both dry and humidified air were adjusted to 0.2 L min^{-1} to obtain the total air flow 0.4 L min^{-1} containing 45–50% humidity. Toluene was injected using a syringe pump in the vertical mixing chamber. The flow rate of the liquid toluene was 0.25 μL min^{-1}. The mixed feed consisted of dry air, humidified air and toluene. The 0.1 g of photocatalyst powder was loaded into the reactor cell for each run. During the preparation period of the mixed gas stream, it flowed from the mixing chamber to the reservoir vessel, through the flow meter and the vent. After steady-state conditions were achieved the feed and the vent were closed and the pump for circulation of the gas stream through the second part of the photoreactor was switched on. The internal flow rate was increased until the catalyst particles were fluidized inside the photoreactor cell. An internal flow rate was usually between 1000 and 1400 mL min^{-1}. The UVA irradiation was started after achieving the adsorption/desorption equilibrium. To prevent heating of the gas stream in the course of photocatalytic reaction, the reservoir was thermostated by a water bath. The temperature of the circulating gas stream was kept at 22 ± 5 °C during each run of 10 h. The concentration of toluene was measured in constant time intervals of reaction. A sample of the gas mixture circulated by a diaphragm pump was injected by an automatic gas valve of the on-line GC–MS. The temperature and relative humidity were checked by the thermometer and the humidity meter (A1-SD1 Sensoren).

2.5. Analytical procedure

The concentration of the toluene was determined on-line by gas chromatography (GC) (Varian 3900) coupled with the mass spectrometer (Varian Saturn 2100 T) operating in an electron impact (EI) mode. The gas samples were injected through a six-port external injection GC valve (Varian CP740641) with a 250 μL automatic sample loop. Then the samples were transferred into a column (Varian CP-Porabound U with the diameter of 0.32 mm and length of 25 m). The gas chromatography was equipped with a split injector. The flow rate of helium as a carrier gas was 1 mL min^{-1}. The injector was held at 250 °C, the oven started at 30 °C, and the temperature was increased with a gradient of 20 °C min^{-1} up to 150 °C and finally maintained constant for 10 min.

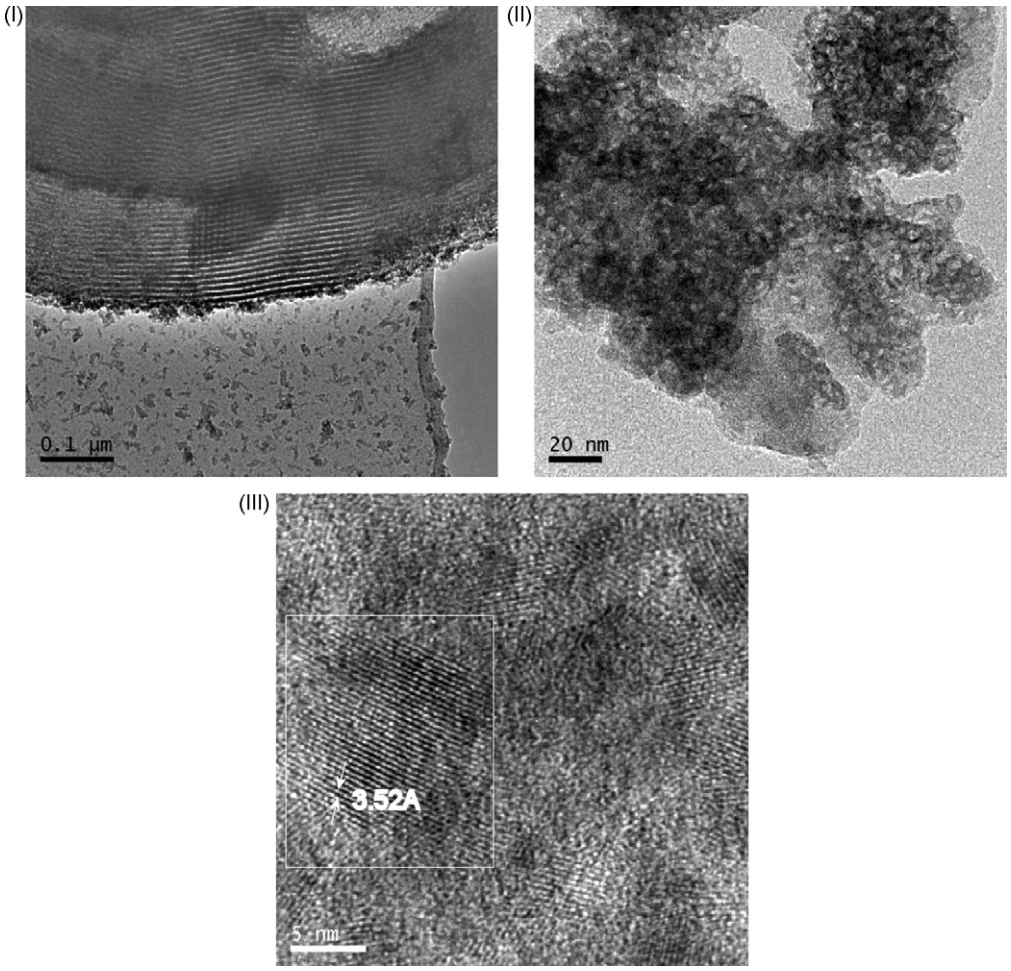

Fig. 2. HR-TEM micrographs of Ti/SBA-15(2/1) powder at different magnifications.

3. Results and discussion

3.1. Structural characteristics of titania/silica photocatalysts

The X-ray diffractograms of Ti/SBA-15(x) and Ti/KIL-2(x) confirm that anatase is the major crystalline phase in both types of samples. The structural properties of the support, ordered mesoporous silica (SBA-15) and disordered mesoporous silica (KIL-2), did not affect the grafting and the growth of nanocrystalline titania in a similar way. The crystallite size of anatase in Ti/KIL-2(x) was slightly lower than that in Ti/SBA-15(x) as reported in Table 1. In addition, the small peak of the brookite phase at $2\theta = 30.8^{\circ}$ was growing while increasing amount of titania [18]. The calculation of crystallite size of anatase in the samples with lower titania loading (Ti/SBA-15(1/2), Ti/SBA-15(1/1) and Ti/KIL-2(1/2)) was not possible due to interference of the (1 0 1) anatase

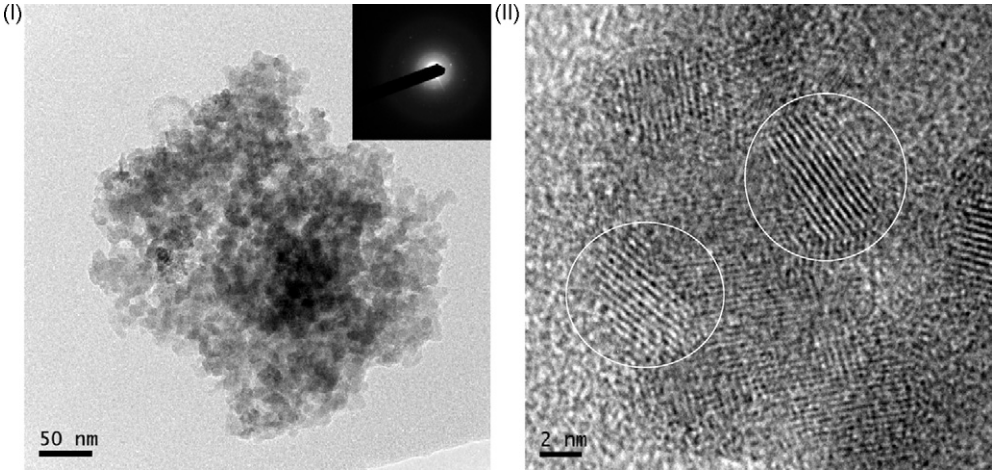

Fig. 3. HR-TEM micrographs of Ti/KIL-2(2/1) powder at different magnifications.

peak with the broad peak of silica. X-ray diffractograms of all prepared samples were measured and compared. They looked similar; the only significant difference was the intensity of the anatase peaks. It was, however, directly proportional to the titania content (more details on XRD results in [14]). Table 1 summarizes the most important physico-chemical characteristics of the samples.

Fig. 2 illustrates HR-TEM micrographs of Ti/SBA-15(2/1) powder at different magnifications. Fig. 2(I) shows an image of Ti/SBA-15(2/1) matrix along (1 1 0) channel directions. The image at higher magnification (Fig. 2(II)) reveals the presence of anatase nanoparticles with the size between 5 nm and 10 nm, slightly lower than estimated by XRD measurement (Table 1). HR-TEM micrograph in Fig. 2(III) shows the lattice image of anatase (PDF 21-1272) confirmed with the d spacing of 3.52 Å corresponding to (1 0 1) plane and tetragonal TiO_2 type cell with space group $I4_1/amd$. The fact that anatase nanoparticles are densely distributed throughout the silica walls with random orientation suggests that they are deposited on the surface of the mesoporous silica matrix rather than incorporated within the silica walls. Wittmann et al. [19] confirmed that the crystalline titania particles appeared on the silica structure when the Ti/Si molar ratio was higher than 0.05. Furthermore, these results are in agreement with our previous work concerning measurements of nitrogen sorption on the same types of powders [14]. We showed that incorporation of titania into SBA-15 led to more narrow pores and decreased surface area of the silicate materials. An increase of Ti/Si molar ratio resulted in a decrease of the surface area of SBA-15 (Table 1). We observed that titania nanoparticles were dispersed inside the channels of SBA-15 when Ti/Si molar ratio was 1/2. Further increase of titania content resulted in a more pronounced growth of titania nanoparticles causing a significant decrease of the open pores [14]. For a Ti/Si molar ratio of 2/1, nanocrystalline titania particles grew also on the external surface of SBA-15.

Fig. 3(I) shows the TEM micrograph of mesoporous silica Ti/KIL-2(2/1) material with textural (interparticle) porosity. The image at higher magnification (Fig. 3(II)) revealed the presence of anatase nanoparticles with an estimated size about 5 nm, confirmed also by XRD measurements (Table 1). Anatase nanoparticles seemed to be deposited on the silica nanoparticles causing only partial blocking of mesopores. This result is also in good agreement with nitrogen sorption measurements described in our previous work [14]. It was concluded that the titania nanoparticles were dispersed inside the pores of KIL-2. This caused narrowing of the pores and decreasing of the surface of KIL-2. For a Ti/Si molar ratio of 2/1, the nanocrystalline titania particles grew on the external surface of KIL-2 silica similar to our observations with SBA-15 silica.

The UV–vis absorption spectra of the samples are shown in Fig. 4. One can see that the spectral edges of Ti/SBA-15(x) and Ti/KIL-2(x) were markedly blue shifted compared to the unsupported TiO_2 (sample Ti1) indicating a smaller size of anatase crystallites in the case of Ti/SBA-15(x) and Ti/KIL-2(x) samples. This result confirms that the incorporation of titania to silica mesoporous materials led to separated nanocrystalline titania particles [20]. In the case of Ti/SBA-15(x) and Ti/KIL-2(x) samples, the spectral edges were shifting blue with decreasing amount of titania (decrease of Ti/Si molar ratio from 2/1 to 1/2). This is in a good agreement with the band-gap energies given in Table 1.

Fig. 5 illustrates FT-IR spectra of all samples. Fig. 5(I) shows the FT-IR spectrum of the sample Ti1 prepared from nanocrystalline aqueous titania sol. The broad band centered at around 3300 cm^{-1} is assigned to the O–H stretching vibration of Ti-OH groups and H_2O molecules [21]. The band at 1622 cm^{-1} belongs to O–H bending vibration of surface adsorbed water [22]. All the sharp bands positioned at 1145 cm^{-1}, 1112 cm^{-1}, 1088 cm^{-1} and 637 cm^{-1} relate to perchlorate [23] and its interaction with titania (TiO_2-perchlorate) [24], which is in agreement with our previous XRD results on the same type of sample confirming the presence of $TiO(ClO_4)_2 \cdot 6H_2O$ [16]. Namely, perchloric acid was used as a peptizing mediator in the synthesis of titania sol. The broad band below 800 cm^{-1} was assigned to the stretching mode of Ti–O–Ti [25]. FT-IR spectra of SBA-15 and Ti/SBA-15(x) are shown in Fig. 5(II) while spectra of KIL-2 and Ti/KIL-2(x) in Fig. 5(III). Spectra of all these samples are similar without any significant differences however, some features can be figured out. In the pure silica samples, the broad bands centered at 3448 cm^{-1} and 3449 cm^{-1} were assigned to O–H stretching vibration of water molecules and Si-OH groups of SBA-15 and KIL-2, respectively. After loading titania, these peaks shifted gradually to lower frequencies (3412 cm^{-1} for Ti/SBA-15(2/1) and 3415 cm^{-1} for Ti/KIL-2(2/1)) due to interaction of silanols with titania. The O–H stretching vibration of Ti-OH groups should also appear at lower frequencies [21,26]. The bands around 1090 cm^{-1} and 800 cm^{-1} were attributed to asymmetric and symmetric stretching vibration of the Si–O–Si framework, respectively [26]. The Si–O–Si stretching vibration at around 1090 cm^{-1} in the samples with titania loading was overlapped with peaks of perchlorate ions. It indicated that perchlorates were not completely removed by washing in the preparation procedure of composite materials. Spectra of SBA-15 and KIL-2 showed bands at 966 cm^{-1} and 970 cm^{-1}, respectively, which were attributed to Si–O stretching vibration of Si-OH groups [27]. Similarly to the shift of O–H stretching vibration described above, also Si-OH vibration gradually shifted to lower frequen-

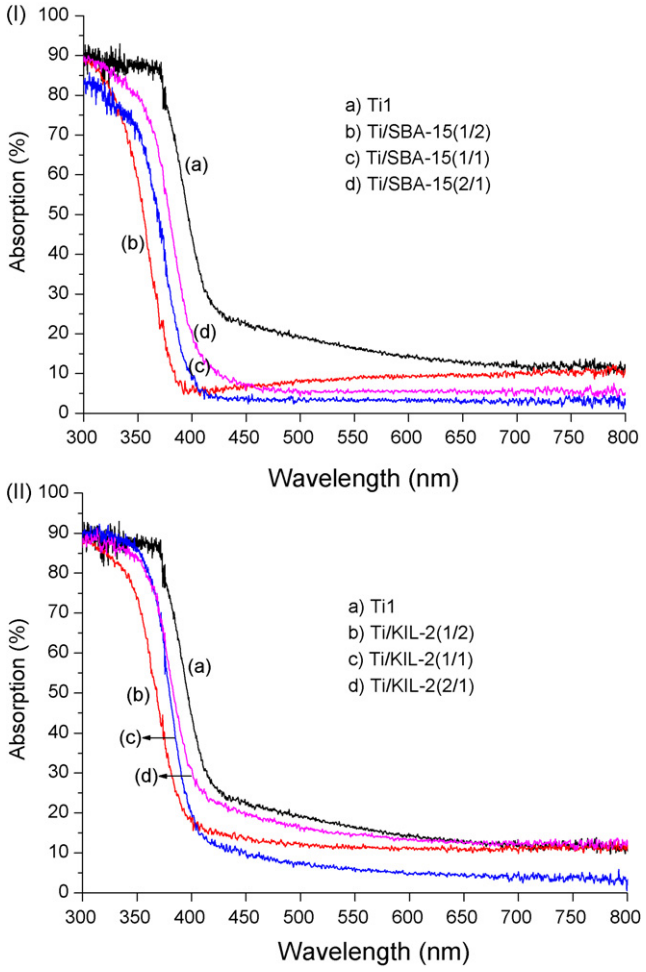

Fig. 4. UV–vis absorption spectra of (I) Ti1, Ti/SBA-15(x) and (II) Ti1, Ti/KIL-2(x).

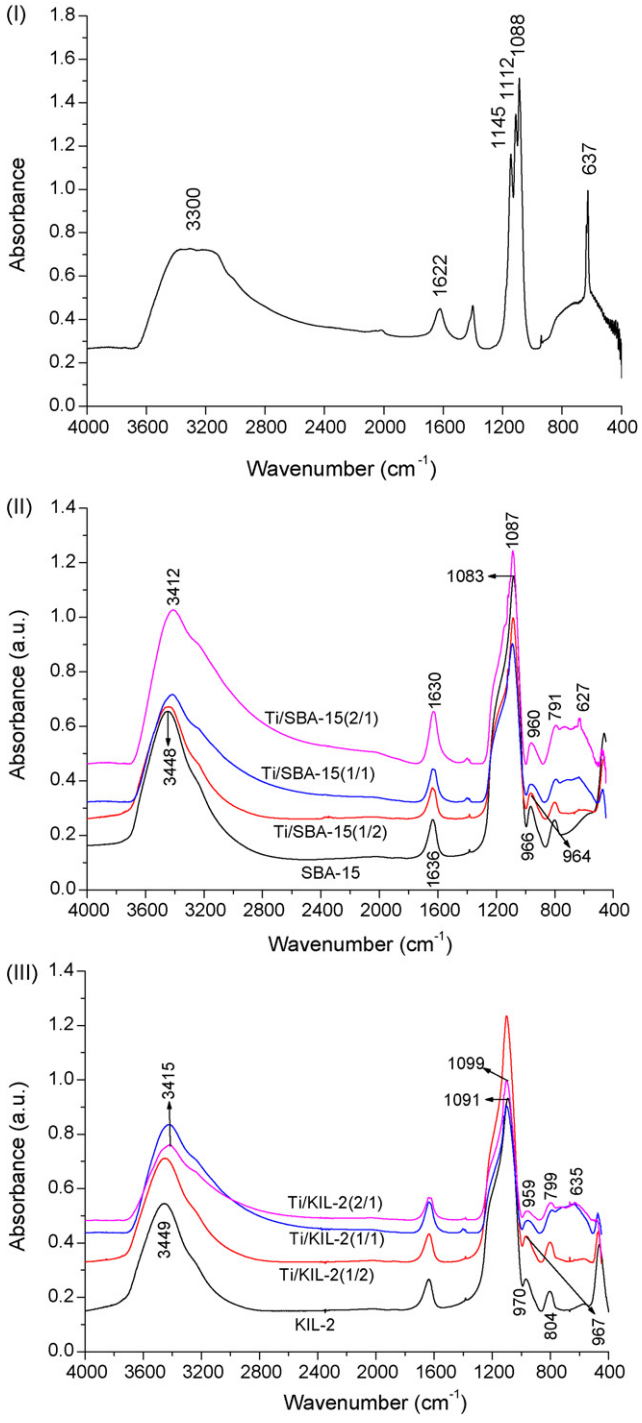

Fig. 5. FT-IR spectra of (I) Ti1, (II) SBA-15, Ti/SBA-15(x) and (III) KIL-2, Ti/KIL-2(x).

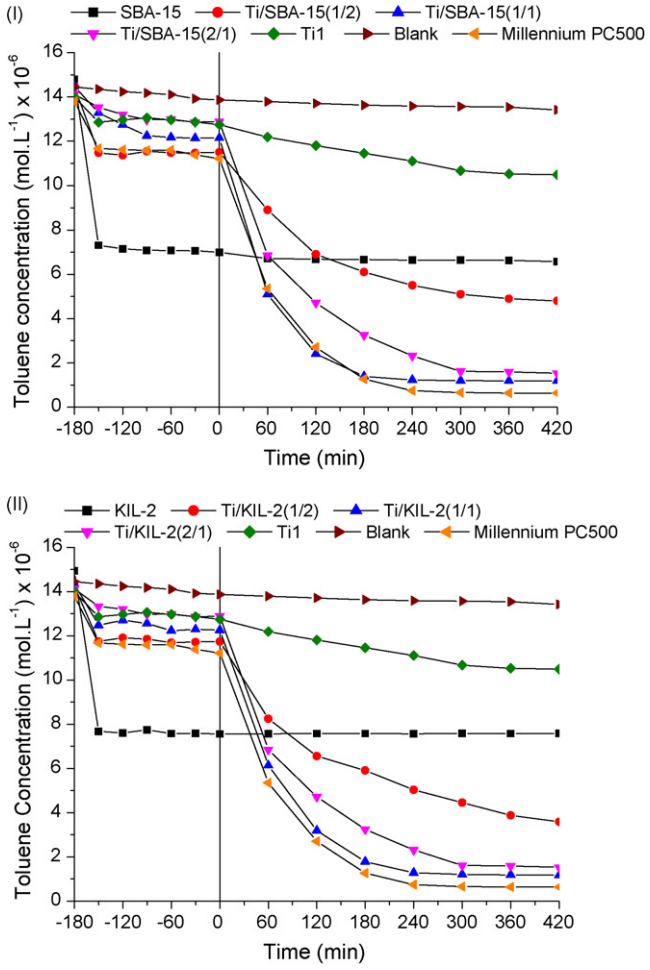

Fig. 6. Concentration of toluene measured prior to and after turning on the UV lamp for (I) blank, Ti1, SBA-15, Ti/SBA-15(x), Millennium PC500 and (II) blank, Ti1, KIL-2, Ti/KIL-2(x), Millennium PC500.

cies with increasing Ti/Si molar ratio, for example, from 964 cm^{-1} to 960 cm^{-1} and from 967 cm^{-1} to 959 cm^{-1} in Ti/SBA-15(x) and Ti/KIL-2(x), respectively. These peaks might also correspond to titanol (Ti-OH) groups and/or the interaction of titania with silanol groups forming Si–O–Ti groups [27,28]. In the case of samples with the higher Ti/Si molar ratio (1/1 and 2/1), a broad Ti–O stretching vibration appeared while for lower Ti/Si molar ratio it was not observed. It could be due to the fact that the growth of titania on external silica surface was promoted after the titania species had been anchored inside the pores of silicate materials (see also discussion above).

3.2. Adsorption of toluene on photocatalyst and photocatalytic activity

The course of adsorption and the photocatalytic degradation of toluene on the synthesized samples are shown in Fig. 6. During the initial dark periods indicated by a negative time scale, adsorption/desorption processes were equilibrated. The rapid disappearance of toluene in the first 30 min corresponded to its adsorption on the surface of particular sample. As one can see in Fig. 6, adsorption properties of different powders were different. In the case of SBA-15 (Fig. 6(I)) nearly 53% of the available toluene was adsorbed while only 8–20% for Ti/SBA-15(x) samples. The highest observed capacity of SBA-15 correlates with the highest surface area of SBA-15 and probably also with its lower polarity compared to Ti/Si samples (Table 1). Adsorption capacities of Ti/SBA-15(x) were decreasing with increasing Ti/Si molar ratio. This corresponds well with the observed negative trend of surface area, which decreased from 560 $m^2\ g^{-1}$ to 336 $m^2\ g^{-1}$ by increasing the Ti/Si nominal molar ratio from 1/2 to 2/1 (Table 1). Adsorption capacity of KIL-2 was also higher compared to the Ti/KIL-2(x) powders and it was again decreasing with increasing Ti/Si molar ratio (Fig. 6(II)). However, adsorption capacity of KIL-2 was lower than that of SBA-15 (approximately 50%) which correlates with their specific surface area (Table 1). Also adsorption capacities of Ti/SBA-15(1/2) and Ti/SBA-15(1/1) were slightly higher than those of Ti/KIL-2(1/2) and Ti/KIL-2(1/1), respectively, in correspondence

with their surface areas (Table 1). However, adsorption capacity of Ti/SBA-15(2/1) and Ti/KIL-2(2/1) were found similar even though the surface area of Ti/SBA-15(2/1) was slightly higher than that of Ti/KIL-2(2/1). Also adsorption capacities of unsupported TiO_2 (sample Ti1) and Ti/SBA-15(2/1) were similar that does not correlate with their surface areas. It can be concluded that the deposition of titania on mesoporous silica lowers surface area of the resulting materials and at the same time specifically affects adsorption of toluene on the surface.

Fig. 6 also shows the photocatalytic period of the experiments (after switching on UVA irradiation at time 0). The concentrations of toluene were decreasing according to first-order reaction (the corresponding rate constants are given in Table 1).

There was no significant disappearance of toluene in the dark experiment carried out without photocatalyst under UV irradiation (blank curve). The small observed decrease of concentration was probably due to a constant leakage of the toluene from the closed loop of the photoreactor system. As expected, the samples of bare mesoporous silica SBA-15 and KIL-2 did not show any photocatalytic activities. There was no absorption of UVA radiation by pure silica as well as no absorption of photons by toluene molecules, therefore no photochemical reactions were possible. As soon as a photocatalyst was added to the system, the photodegradation of toluene occurred. Photocatalytic degradation of toluene on Ti1 proceeded more slowly compared to titania immobilized on silica. As an example, Ti1 and Ti/SBA-15(2/1) can be compared. They showed similar dark adsorption but the photocatalytic degradation of toluene proceeded 11 times faster in case of immobilized titania (Ti/SBA-15(2/1)). The results of photocatalytic measurements cannot be simply explained by taking into account only the amount of titania present in the reactor cell (the calculated amount of titania for the particular samples is reported in Table 1). In photocatalysis not only the amount of the powder is important, but also many other parameters prevail. The observed lower photocatalytic activity of unsupported titania could be caused by the aggregation of titania nanoparticles in the absence of the silica support that might reduce the direct contact of gaseous molecules of toluene on the surface of TiO_2 nanoparticles. In this way the realized immobilization was found beneficial for our gaseous photocatalytic system.

In the case of SBA-15 and KIL-2 supports, the highest photocatalytic performance showed for samples with the Ti/Si molar ratio 1/1. It should be remembered in this respect that a constant amount of 0.1 g of the photocatalyst powder was loaded into the reactor cell for each experiment independently of the Ti/Si molar ratio. It means at the same time that the amounts of TiO_2 present in the reaction system depended on the Ti/Si nominal molar ratio as given in Table 1. In spite of this fact, the following explanation of the observed trend could be proposed. The silica surface was not completely covered by titania in 1/2 composites. That is why their photoactivity was lower compared to 1/1 composite, where the covering of silica surface by titania was higher. When the amount of titania was additionally increased in the 2/1 composite, aggregation of titania on silica surface already occurred causing the observed reduction of the photocatalytic performance. One could expect that the photoactivity would become similar to that unsupported titania (Ti1) if more titania is additionally loaded.

The intermediates which are adsorbed on the surface of photocatalyst in the photocatalytic degradation of toluene depend on the reaction parameters, especially the relative humidity (RH) of the reaction environment. Sleiman et al. [29] found that benzaldehyde, benzoic acid, and traces of benzene and formic acid are formed on the surface of TiO_2 PC500 (100% anatase) at high and low RH level. In our case the only gaseous by-product, which was detected, was CO_2, which is the final degradation product of toluene oxidation, but the quantitative measurements of evolved CO_2 were not done.

The color of the powders was changed after photocatalytic reaction tests. It was probably associated with an accumulation of polycondensed aromatic intermediates on the photocatalyst surface according to the results published in [30]. The color of Ti/SBA-15(1/2) and Ti/KIL-2(1/2) changed less than that of Ti/SBA-15(1/1) and Ti/KIL-2(1/1), which became a light yellow. The color of samples with the Ti/Si molar ratio 2/1 was even more yellowish despite the slower toluene photodegradation. To obtain more detailed information, an analysis of the organics deposit needs to be performed. The color of the Ti1 catalyst changed from cream to light brown upon irradiation that might also be due to accumulation of polycondensed aromatic intermediates [30]. One of the possible explanations for differences in color appearance could be the presence of silica. The deposited intermediates degraded faster on titania, which is in a close proximity to silica (maybe silica prevents the deposition of multilayers of organic intermediates). Therefore the unsupported titania (sample Ti1) and 2/1 supported titania changed the color the most dramatically.

For comparison of our samples with commercial photocatalysts, a Millennium PC500 was chosen since it had a comparable BET surface area and similar fluidization behavior in the reactor cell as our materials. Adsorption capacity of Millennium PC500 was comparable to that of our samples with Ti/Si molar ratio 1/2, however, its photocatalytic performance was as high as for the samples which were prepared by Ti/Si molar ratio 1/1. It should be mentioned that PC500 is, as a highly crystalline material, a better photocatalyst than our unsupported titania prepared by a low-temperature synthesis. Therefore its faster reaction of toluene degradation compared to low-temperature prepared titania was not surprising. Nevertheless, we showed that even low-temperature titania can become highly photoactive when adsorbed to an appropriate substrate.

4. Conclusions

Titania/mesoporous silica photocatalysts were synthesized via the sol–gel impregnation method with different Ti/Si nominal molar ratios (1/2, 1/1 and 2/1). Aqueous nanocrystalline titania sol was used as a photoactive component while silica mesoporous materials were employed as high-surface-area supports. The photocatalytic activity of as-prepared powders was investigated towards photocatalytic degradation of gaseous toluene in a fluidized-bed photoreactor which was constructed for this purpose. The effects of Ti/Si molar ratio and of mesoporous silica structure were investigated measuring adsorption capacity and photocatalytic degradation of toluene. The results revealed that Ti/Si molar ratio is more important compared to structural properties of the mesoporous silica support. By incorporation of aqueous titania sol into mesoporous silica support, the nanocrystalline titania particles are separately distributed on silica surface. Increasing Ti/Si molar ratio led to a decrease in surface area as well as adsorption capacity for both types of mesoporous silica supports. Photocatalytic performance reached the maximum when the Ti/Si nominal molar ratio was 1/1.

Acknowledgements

This research was supported by the Ministry of Higher Education, Science and Technology of the Republic of Slovenia. We are very grateful to Dr. Martin O'Loughlin for English revision of the manuscript.

References

[1] H.J. Seinfeld, S.N. Pandis, Atmospheric Chemistry and Physics, John Wiley & Sons Inc., New York, 1998.
[2] T. Oppenlander, Photochemical Purification of Water and Air, Wiley–VCH, 2003.

[3] O. Prieto, J. Fermoso, R. Irusta, Int. J. Photoenergy (2007), doi:10.1155/2007/32859, Article ID 32859.
[4] H.P. Kuo, C.T. Wu, R.C. Hsu, Powder Technol. 195 (2009) 50–56.
[5] K. Sekiguchi, K. Yamamoto, K. Sakamoto, Catal. Commun. 9 (2008) 281–285.
[6] M. Kang, W.-J. Hong, M.-S. Park, Appl. Catal. B: Environ. 53 (2004) 195–205.
[7] M.V. Chandak, Y.S. Lin, Environ. Technol. 19 (1998) 941–948.
[8] X.S. Zhao, Q. Ma, G.Q.M. Lu, Energy Fuel 12 (1998) 1051–1054.
[9] C.W. Kwong, C.Y.H. Chao, K.S. Hui, M.P. Wan, Atmos. Environ. 42 (2008) 2300–2311.
[10] T. Ibusuki, K. Takeuchi, Atmos. Environ. 20 (1986) 1711–1715.
[11] L. Zou, Y. Luo, M. Hooper, E. Hu, Chem. Eng. Process. 45 (2006) 959–964.
[12] J. Mo, Y. Zhang, Q. Xu, R. Yang, J. Hazard. Mater. 168 (2009) 276–281.
[13] M. Popova, A. Szegedi, P. Nemeth, N. Kostova, T. Tsoncheva, Catal. Commun. 10 (2008) 304–308.
[14] M. Tasbihi, U. Lavrenčič Štangar, A. Sever Škapin, A. Ristić, V. Kaučič, N. Novak Tušar, J. Photochem. Photobiol. A: Chem. (2010), doi:10.1016/j.jphotochem.2010.07.011.
[15] N. Novak Tušar, A. Ristić, G. Mali, M. Mazaj, I. Arčon, D. Arčon, V. Kaučič, N. Zabukovec Logar, Chem. Eur. J. 16 (2010) 5783–5793.
[16] M. Tasbihi, U. Lavrenčič Štangar, U. Černigoj, K. Kogej, Photochem. Photobiol. Sci. 8 (2009) 719–725.
[17] K. Kočı, L. Obalova, L. Matejova, D. Placha, Z. Lacny, J. Jirkovsky, O. Šolcova, Appl. Catal. B: Environ. 89 (2009) 494–502.
[18] U. Lavrenčič Štangar, U. Černigoj, P. Trebše, K. Maver, S. Gross, Monatsh. Chem. 137 (2006) 647–655.
[19] G. Wittmann, K. Demeestere, A. Dombi, J. Dewulf, H. Van Langenhove, Appl. Catal. B: Environ. 61 (2005) 47–57.
[20] J. Yang, J. Zhang, L. Zhu, S. Chen, Y. Zhang, Y. Tang, Y. Zhu, Y. Li, J. Hazard. Mater. B137 (2006) 952–958.
[21] M. Kanna, S. Wongnawa, Mater. Chem. Phys. 110 (2008) 166–175.
[22] M. Nag, P. Basak, S.V. Manorama, Mater. Res. Bull. 42 (2007) 1691–1704.
[23] J.M. Janik, G. Pytasz, T. Stanek, Acta Phys. Pol. XXXV (1969) 997–1008.
[24] A.J. McQuillan, Adv. Mater. 13 (2001) 1034–1038.
[25] M.J. Velasco, F. Rubio, J. Rubio, J.L. Oteo, Thermochim. Acta 326 (1999) 91–97.
[26] H. Ding, H. Sun, Y. Shan, J. Photochem. Photobiol. A: Chem. 169 (2005) 101–107.
[27] S. Perathoner, P. Lanzafame, R. Passalacqua, G. Centi, R. Schlogl, D.S. Su, Microp. Mesopor. Mater. 90 (2006) 347–361.
[28] M.R. Boccuti, K.M. Rao, A. Zecchina, G. Leofanti, G. Petrini, Stud. Surf. Sci. Catal. 48 (1989) 133–144.
[29] M. Sleiman, P. Conchon, C. Ferronato, J.-M. Chovelon, Appl. Catal. B: Environ. 86 (2009) 159–165.
[30] E. Barraud, F. Bosc, D. Edwards, N. Keller, V. Keller, J. Catal. 235 (2005) 318–326.